Journal of Catalysis 269 (2010) 229–241

Contents lists available at ScienceDirect

Journal of Catalysis

journal homepage: www.elsevier.com/locate/jcat

Building MOF bottles around phosphotungstic acid ships: One-pot synthesis of bi-functional polyoxometalate-MIL-101 catalysts

Jana Juan-Alcañiz, Enrique V. Ramos-Fernandez, Ugo Lafont, Jorge Gascon *, Freek Kapteijn

Catalysis Engineering, DelftChemTech, Delft University of Technology, Julianalaan 136, 2628 BL Delft, The Netherlands

ARTICLE INFO

Article history:
Received 14 September 2009
Revised 5 November 2009
Accepted 10 November 2009
Available online 16 December 2009

Keywords:
Metal organic frameworks
MIL-101
Polyoxometalates
Phosphotungstic acid
Knoevenagel condensation
Esterification
Etherification
Encapsulated catalyst
Bi-functional catalyst

ABSTRACT

A new strategy has been developed for the direct encapsulation of polyoxometalates (POMs) into MIL-101(Cr). The addition of phosphotungstic acid (PTA) to the synthesis mixture of MIL-101 yields the direct encapsulation of chromium-containing polyoxometalates (POMs) inside the MOF structure, with a good distribution over the MIL-101 crystals. Vibrational Spectroscopy (DRIFT, Raman, UV–Vis) reveals the partial substitution of tungsten by Cr^{3+} resulting in the so-called lacunary structures, which are highly active in catalysis.

The medium-sized cavities of MIL-101 are occupied by POM units bigger than their pentagonal windows when this one-pot approach is followed, and no leaching is observed.

These new catalysts show the highest activities reported to date at 313 K for the Knoevenagel condensation of benzaldehyde with ethyl cyanoacetate when using apolar toluene as solvent as well as when using polar DMF and ethanol, with TOFs exceeding 600 h^{-1}. In addition, they exhibit a remarkable activity in two acid-catalyzed reactions, the esterification of *n*-butanol with acetic acid in liquid phase slurry operation and the dimethyl ether production from methanol in a fixed bed gas phase operation, in contrast to the poor or absent activity of the catalysts prepared via the impregnation of the polyoxometalate in MIL-101, where the strong interaction between POM and support deteriorates the catalytic performance.

1. Introduction

Metal organic frameworks (MOFs) have attracted the attention of scientists all around the world during the last decades, resulting in an unprecedented explosion of publications in the topic. The combination of organic and inorganic subunits on fully crystalline porous materials has led to a vast chemical versatility, giving rise to more than 10000 MOF structures [1].

Considering the number of structures discovered, it must be realized that only a limited number of applications of these materials has been investigated. As reviewed very recently, research is focused mainly on the discovery of new structures [2–4] together with the characterization and identification of features like luminescence [5], or magnetic properties [6], while only a small percentage of the more than 1000 papers published every year on MOFs deal with specific applications. Among them, gas storage [7] and adsorptive separation [8,9] are the most studied.

Heterogeneous catalysis using MOFs is still in an immature state [10], being one of the most underdeveloped areas of the MOF research, as pointed out by Lee et al. [11]. Up to now, mainly proofs of principle related to catalysis on MOFs have been reported [12–18]. Serious catalytic studies, including long-term utilization and screening of different reaction conditions are still scarce [19–23]. This may be attributed to two main reasons. First the continuous *runaway* status of MOF chemistry is a strong driving force for proof of principle publishing, usually leading to incomplete works. Second, the use of MOFs in catalysis has been largely hampered by their relatively low thermal and chemical stability. In this sense, the MOF community is indebted to Ferey's group for discovering thermally and chemically robust structures [24–27]. The development of such structures provides an excellent playground for heterogeneous catalysis that has yet hardly been explored.

Indeed, materials like MIL-101 offer tremendous possibilities for catalyst engineering. This hybrid solid is built up from *super-tetrahedra* (ST) building units, which are formed by rigid terephthalate ligands and trimeric chromium (III) octahedral clusters. The resulting solid owns two types of quasi-spherical mesoporous cages limited by 12 pentagonal faces for the smaller and by 16 faces for the larger. The so-called medium cavities are accessible through 1.2 nm pentagonal windows, while the large cavities are communicated through the same pentagonal windows and 1.5 nm hexagonal windows (Fig. 1) [24].

The presence of coordinatively unsaturated metal sites (CUS) in MIL-101 allows their use as a mild Lewis acid and, more importantly, allows their post-functionalization via grafting of active

* Corresponding author.
E-mail address: j.gascon@tudelft.nl (J. Gascon).

0021-9517/$ - see front matter © 2009 Elsevier Inc. All rights reserved.
doi:10.1016/j.jcat.2009.11.011

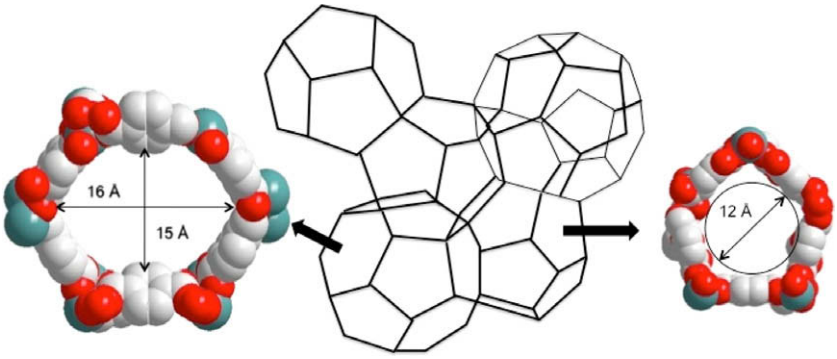

Fig. 1. MIL-101(Cr) structure. (Left) Hexagonal windows; (center) zeotype structure; and (right) pentagonal windows. Red: oxygen; green: chromium; and white: carbon. (For interpretation of the references to colour in this figure legend, the reader is referred to the web version of this article.)

species. In pioneering work, Jhung and coworkers demonstrated the possibility of post-functionalization of the MIL-101 framework with different amines and applied the obtained basic catalyst in a Knoevenagel condensation and for immobilizing metals [28]. The zeotype cavities of two different sizes, the fully accessible porosity, and therefore outstanding sorption properties, together with a high thermal and chemical stability make MIL-101 an excellent candidate for supporting catalytic species. In this sense mainly two post-synthetic approaches have been followed: the deposition of Pd nanoparticles for the use of MIL-101 in hydrogenation reactions [29] and the impregnation of polyoxometalate anions in the large cavities for their later use as an oxidation catalyst [21].

Polyoxometalates (POMs) present several advantages as catalysts that make them economically and environmentally attractive [30]. POMs are complex Brønsted acids that consist of heteropolyanions having metal-oxygen octahedra as the basic structural units. The first characterized and the best known of these is the Keggin heteropolyanion, typically represented by the formula $XM_{12}O_{40}^{x-8}$ where X is the central atom. With a very strong Brønsted acidity, approaching the superacid region, and exhibiting fast reversible multi-electron redox transformations under rather mild conditions, POMs represent a serious alternative to other acid systems. Their acid–base and redox properties can be varied over a wide range by changing the chemical composition. This unique structure exhibits extremely high proton mobility, while heteropolyanions can stabilize cationic organic intermediates. On top of that POMs have a good thermal stability in the solid state, far better than other strong acids like ion exchange resins [30].

Supporting POM catalysts is important for applications because bulk POMs have a low specific surface (1–5 m^2/g). Acidic or neutral substances such as SiO_2, Al_2O_3, and activated carbons have been explored as carriers [31–35]. The acidity and catalytic activity of the supported POMs depend mainly on the type of carrier and on the loading, i.e. the interaction with activated carbons is so strong that the activity of the final catalyst is much lower than that of the POM itself, while low interactions of POM–support lead to dramatic leaching. Encapsulation of POMs inside zeolitic cavities has been achieved by direct synthesis of the Keggin structures inside the zeolite cavities (FAU). This approach is shown to solve the problem of leaching, since the POM clusters are bigger than the windows of the zeolitic cavities, but only very low loadings can be utilized (<5 wt%) if diffusion limitations are to be avoided [36].

As explained before, polyoxometalates with the Keggin structure have been impregnated into the large cavities of MIL-101. Lacunary $PW_{11}O_{40}^{7-}$ anions (one tungsten less than Keggin ion) were introduced in order to demonstrate the large volume of such large cavities [24]. Following a similar approach, Maksimchuk et al. impregnated different Ti and Co Keggin anions into the large cavities of MIL-101 and the catalytic performance of the resulting materials was assessed in the oxidation of three representative alkenes using molecular oxygen and aqueous hydrogen peroxide as oxidants. The catalysts could be reused several times without significant activity losses and they were shown to be stable under mild operation conditions [21]. Very recently, a series of HPAs were encapsulated by means of a one-step hydrothermal reaction of copper nitrate, benzene 1,3,5 tricarboxylate (BTC), and different Keggin polyoxometalates. In these compounds, the catalytically active Keggin polyanions were alternately arrayed as noncoordinating guests in the cubo-octahedral cages of a Cu-BTC MOF host matrix (HKUST-1), showing activities similar to that of the bare acid in the hydrolysis of some esters, although diffusion limitations seem to be a problem in the case of CuBTC due to the comparable size of the Keggin anions and the large cavities of this MOF [18].

In the case of MIL-101, the impregnation approach has been demonstrated to be successful, but only the large cavities of MIL-101 can be accessed by Keggin-like structures (13–14 Å diameter). Taking into account that the medium-sized cavities represent 2/3 of the total number of cavities in MIL-101 and that the window openings of these cavities are smaller than those of the Keggin structures, it is obvious that the encapsulation of such active species into the medium cavities would offer many advantages, like a better dispersion and utilization of the support. Moreover, if contained in the medium cavities, leaching of the polyoxometalates would never be a problem, since they are bigger than the windows of these cavities.

In this work, we present a new, direct synthetic encapsulation of active species into MOFs [12,18]. We demonstrate that it is possible to incorporate highly dispersed POMs into MIL-101 by following a one-pot synthesis approach. Moreover, we show that the interaction of Cr^{3+} ions with phosphotungstic acid during the encapsulation process results in the stabilization of lacunary POMs due to the exchange of tungsten by Cr^{3+}. In addition to a complete characterization of the POM encapsulated samples, their catalytic performance is shown for reactions involving proton-abstraction (Knoevenagel), liquid phase acid-catalyzed esterification (acetic acid with *n*-butanol) and gas phase acid-catalyzed etherification (methanol dehydration).

2. Experimental

2.1. General information

All chemicals were obtained from Sigma–Aldrich and were used without further purification. High resolution transmission electron microscopy (HRTEM) on a Philips CM30T (150–300 kV) microscope

was used to determine crystal morphology and size of the new MOF as well as the dispersion of the POMs. In order to probe the interior of the crystals, cryo-slicing was applied. Briefly, a dispersion of MOF crystals in ethanol was frozen with liquid N_2, ensuring minimal disturbance of the structure of the catalysts. The frozen catalyst samples were subsequently sectioned into 0.2 mm slices that present a better stability under the HRTEM beam. Although this technique has been widely applied in life sciences, this example represents, to the best of our knowledge, its first application to MOFs.

Scanning Electron Microscopy (SEM) was measured in a JEOL JSM 6500F setup coupled to an Energy Dispersive Spectrometer (EDS) for micro-analysis.

Nitrogen adsorption at 77 K in a Quantachrome Autosorb-6B unit gas adsorption analyzer was used to determine the textural properties as BET surface area between 0.05 and 0.15 relative pressures and pore volume at 0.95 relative pressures. The crystalline structures were analyzed by X-ray diffraction (XRD) using a Bruker-AXS D5005 with CuKα radiation. Thermogravimetric analysis (TGA) of the MOFs was performed by means of a Mettler Toledo TGA/SDTA851e, under flowing 60 ml/min of air at heating rates of 10 K/min up to 873 K.

Elemental analysis was carried out by means of Inductively Coupled Plasma Optical Emission Spectroscopy (ICP-OES). The samples were digested in duplo in a mixture of 1% HF and 1.25% H_2SO_4 and were analyzed with an ICP-OES Perkin Elmer Optima 3000 dv in order to determine the amount of POM present in the structure.

DRIFT spectra were recorded in a Bruker model IFS66 spectrometer, equipped with a high-temperature cell with CaF_2 windows and a 633 nm laser. The spectra were registered after accumulation of 128 scans and a resolution of 4 cm^{-1}. A flow of helium at 10 ml/min was maintained during the measurements. Before collecting the spectra, the different samples were pretreated in a helium flow at 393 K for 30 min. KBr was used as background.

The laser Raman spectra were obtained by using a Renishaw Raman imaging microscope, system 2000. The green (l = 514 nm) polarized radiation of an argon-ion laser beam of 20 mW was used for excitation. A Leica DMLM optical microscope with a Leica PL floutar L500/5 objective lens was used to focus the beam on the sample. The Ramascope was calibrated using a silicon wafer. Samples were dehydrated in situ in an air flow of 100 ml/min, by using a temperature programed heated cell (Linkam TS1500). Spectra were collected in the range 100–2000 cm^{-1}.

UV–Vis/NIR Diffuse Reflectance spectra were measured with a Perkin–Elmer Lambda 900 spectrophotometer equipped with an integrating sphere (“Labsphere”) in the 200–800 nm range. The Kubelka–Munk function was used to convert reflectance measurements into equivalent absorption spectra using the reflectance of $BaSO_4$ as a reference, and to obtain absorption edge energies directly from the curves.

2.2. Catalysts syntheses

The synthesis of the MIL-101(Cr) catalysts was adapted from the literature [24,37]. Phosphotungstic Acid ($H_3PW_{12}O_{40}{\cdot}xH_2O$, abbreviated as H_3PW) was added during the synthesis or impregnated on activated (evacuated) MIL-101 as explained later. The resulting MOFs are referred to as MIL-101$(Cr)_{ENCAPSULATED}$ or MIL-101$(Cr)_{IMPREGNATED}$.

2.2.1. MIL-101(Cr)

For the synthesis of MIL-101(Cr) a mixture of 1.63 g of chromium (III) nitrate, $Cr(NO_3)3{\cdot}9H_2O$ (97%), 0.7 g of terephthalic acid, C_6H_4-1,4-$(CO_2H)_2$ (97%), 0.20 g of hydrofluoric acid, HF (40%), and 20 g of distilled water, H_2O, was added in a Teflon container inside an autoclave. Then the autoclave was heated for 8 h at 493 K in an oven under static conditions.

Once the synthesis was completed, the solid product was doubly filtered off using two glass filters with a pore size between 40 and 100 μm to remove the free terephthalic acid. Then a solvothermal treatment was sequentially performed using ethanol (95% EtOH with 5% H_2O) at 353 K for 24 h. The resulting solid was soaked in 1M of ammonium fluoride, NH_4F, solution at 343 K for 24 h and was immediately filtered and washed with hot water. The solid was finally dried overnight and stored at 433 K under air atmosphere.

2.2.2. MIL-101$(Cr)_{ENCAPSULATED}$

The encapsulation of the polyoxometalate follows the same procedure as followed in the previous case (MIL-101(Cr)) with respect to the synthesis mixture and cleaning. However the phosphotungstic acid (H_3PW) was added to the Teflon container with the rest of the mixture.

Two different types of syntheses were tested: under static conditions at 493 K or while rotating the autoclave at 473 K, and in both cases for 8 h.

Depending on the amount of H_3PW introduced into the synthesis mixture, catalysts with different loadings were obtained (50 wt% and 20 wt% according to elemental analysis). Usually, 80% of the H_3PW added to the synthesis vessel was incorporated into the MOF, while the rest was filtered off together with the mother liquor.

2.2.3. MIL-101$(Cr)_{IMPREGNATED}$

The adsorption of the polyoxometalate is performed once the MIL-101(Cr) is synthesized and activated following the procedure described before. The adsorption was performed following the procedure described by Ferey et al. [24]: mixing 100 mg of H_3PW and 100 mg of the MIL-101(Cr) sample with 10 mL of distilled water in an Erlenmeyer flask at room temperature and under stirring for 12 h. In addition, the samples containing half of the H_3PW amount, 50 mg, were prepared following a similar procedure.

2.3. General procedure for the catalytic test reactions

2.3.1. Knoevenagel condensation

In a typical batch experiment, 0.5 g of catalyst was added under stirring to a solution of 7 mmol ethyl cyanoacetate (ECA) in 5 mL of toluene as a solvent in an Erlenmeyer flask at 313 K. After temperature adjustment, benzaldehyde (8 mmol) was added.

Reference experiments (blank runs) were performed. External agitation (shaking) was used instead internal stirring in order to avoid attrition of the particles and to facilitate the reuse of the different catalysts. After recovering the catalyst, it was filtered, stored at 423 K and reused.

1,5,7-Triazabicyclo[4.4.0]dec-5-ene (Sigma–Aldrich) was used as a homogeneous organocatalyst under the same conditions in order to benchmark the activity of the synthesized MOF catalyst with a well-known strong base (0.2 mmol of catalyst).

2.3.2. Esterification of acetic acid and n-butanol

The esterification of acetic acid and *n*-butanol was performed without solvent using a molar ratio acetic acid: *n*-butanol = 1:1. The mixture was introduced in a balloon flask, while being stirred under reflux at 383 K. A ratio of 3 g catalyst per mol of HAc was used.

Nafion NR50 was used to benchmark the acidity of the resulting catalysts. After recovering the catalyst, it was filtered, stored at 423 K, and reused.

In both Knoevenagel and esterification experiments, the samples of the reaction mixture were periodically analyzed by gas chromatography using a Chrompack GC CP-Sil 8CB Cat. No. 7453

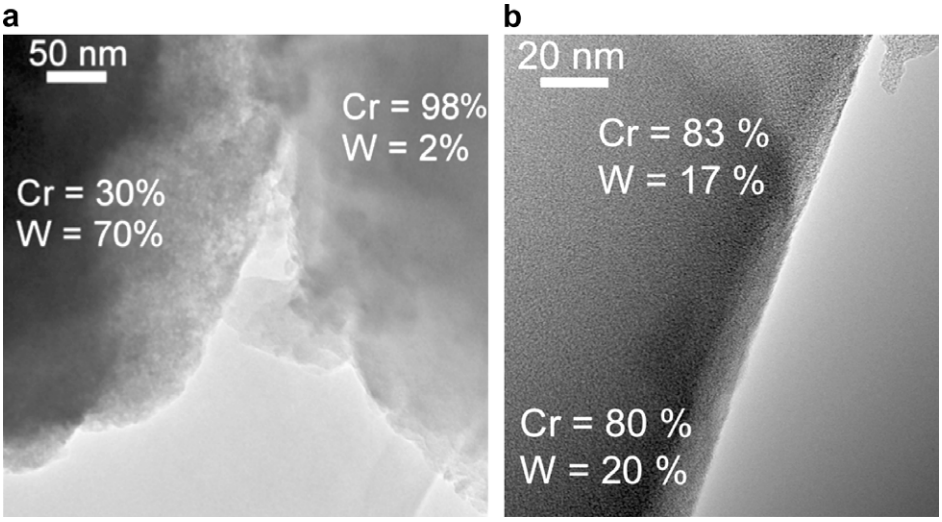

Fig. 2. High-Resolution Transmission Electron Microscopy (HRTEM) images and EDX mapping of the 50 wt% encapsulated POM. (a) Static synthesis and (b) rotational synthesis.

equipped with an FID detector and a 50 m RTX®-1 (1% diphenyl-, 99% dimethylpolysiloxane) fused silica capillary column. The analysis was carried out directly after sampling to avoid any additional conversion in the reaction mixture.

TOFs and TONs were based on the total number of Keggin units (PW_{12}) present in each catalyst (as obtained from elemental analysis), and TOFs were calculated from the first reaction data points in the batch experiments.

2.3.3. Dehydration of methanol

The dehydration of methanol to dimethyl-ether (DME) was carried out in gas phase. Experiments were performed in a 1/4 in. stainless steel reactor with a length of 2 cm. Pressed catalyst (0.1 g) with a mesh size around 0.75–1 mm was loaded in the reactor. Quartz wool was placed on the top the bed for better packing of the catalyst in the reactor. An ISCO liquid pump was used to feed the liquid methanol to the reactor together with N_2 (5.6 or 9.16 mL/min) by a mass flow controller. Methanol was fed to the reactor at a flow rate of 0.25, 0.5, and 1 mL/h resulting in WHSV range of 2–8 h^{-1}. The temperature of the reactor was varied between 523 and 643 K. The pressure drop over the reactor was around 0.25 bar. The product mixture was analyzed online with an Interscience Compact GC over a 50 m RTX®-1 (1% diphenyl-, 99% dimethylpolysiloxane) column at 300 K.

3. Results

3.1. Characterization of the catalysts

3.1.1. Static vs. rotating synthesis by HRTEM

Fig. 2 shows the comparison between 2 HRTEM micrographs corresponding to two samples synthesized under static and rotating conditions, respectively, together with an EDX analysis in different areas of the crystals. The dispersion of the tungsten in the samples prepared under static conditions is very inhomogeneous; the concentration of tungsten in some particles is really high, while other crystals do not contain any (Fig. 2a). In contrast, when applying rotating conditions, a homogeneous distribution of tungsten over the particles can be observed (Fig. 2b).

Consequently, rotating synthesis was applied as standard and all further results presented correspond to the samples synthesized under these conditions.

In Fig. 3 a comparison between two cryo-sliced samples of encapsulated POM and bare MIL-101 is made. An excellent dispersion of the complex within the cavities of MIL-101 is reached through encapsulation, with most of the POM present in the interior of the crystals, as shown by the difference in contrast between the edge and the core of the particles.

3.1.2. SEM + Energy Dispersive Spectroscopy (EDS)

Fig. 4 shows the EDS mapping of different elements in the MIL-101(Cr) with 20 wt% encapsulated catalyst. The good distribution of all the elements analyzed is in agreement with the TEM results.

3.1.3. Nitrogen adsorption: BET surface, pore volume and isotherms

Table 1 shows the BET surface area and total pore volume of the different MOFs, on a mass basis and calculated per gram of MIL-101 (values in parentheses), while the adsorption isotherms normalized by the uptake at a relative pressure of 0.4 are shown in

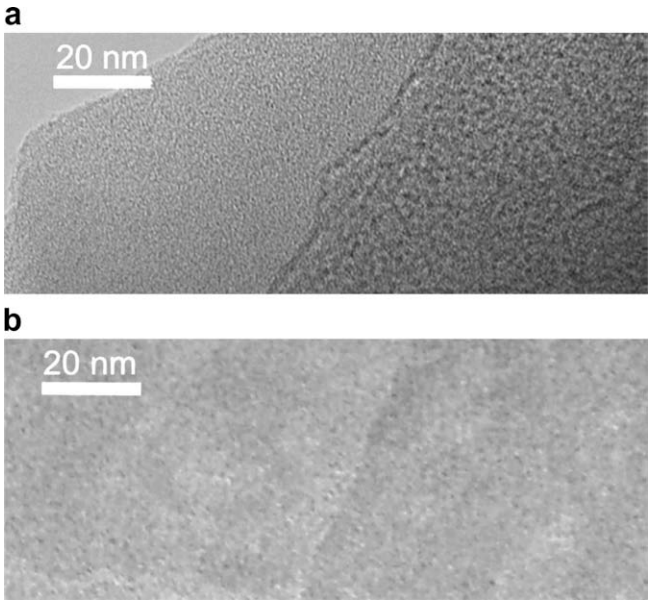

Fig. 3. HRTEM micrographs of two cryo-sliced samples: (a) MIL-101(Cr) and (b) MIL-101(Cr) with 20 wt% of POM encapsulated.

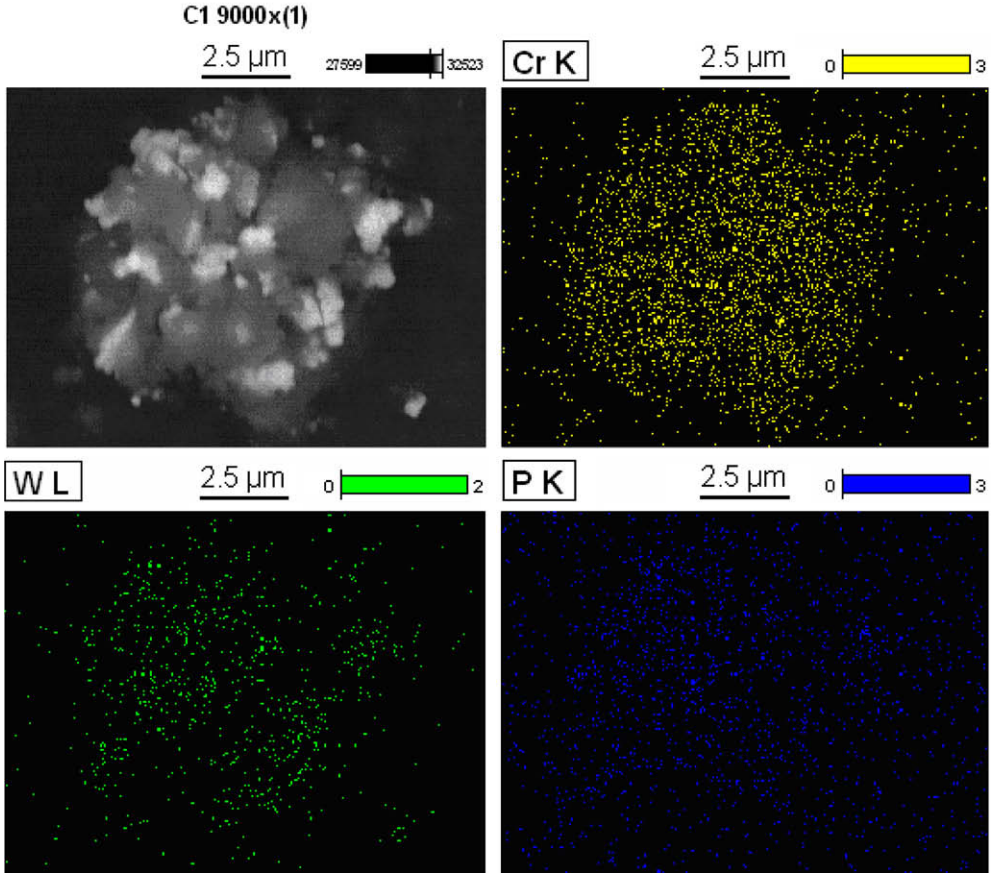

Fig. 4. EDS analysis on MIL-101(Cr) with 20 wt% of POM encapsulated.

Fig. 5. In the case of MIL-101(Cr) the BET surface area is smaller than values reported in the literature [24]. The deviation may be explained by the choice of the pressure region used for the BET calculation, in this study between 0.05 and 0.15 relative pressure, since the BET surface area should be calculated before the two characteristic steps in the isotherm of this material appearing at P/P^0 = 0.15 and 0.20 corresponding to the filling of the two different cavities of the MIL-101 [24]. The stepwise filling of such cavities should not be included in the calculation of the BET area.

The encapsulated samples show a BET surface area per total amount of sample similar to the bare sample of MIL-101(Cr) used as a reference, while a more important decrease is observed in the case of the adsorption modified sample. Interestingly when comparing the BET values per gram of MOF, the area of the impregnated samples is similar to that of MIL-101, while the encapsulated samples show a much higher specific surface area.

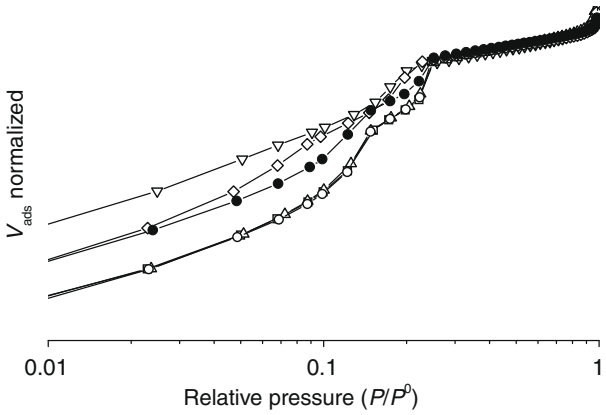

Fig. 5. N_2 adsorption isotherms of different catalysts normalized at uptake at 0.4 relative pressure. Key: (□) MIL-101(Cr); (●, ○, △) MIL-101(Cr) encapsulated with POM 10, 20, and 50 wt%, respectively; (▽, ◇) MIL-101(Cr) with POM 30 wt% and 50 wt% impregnated, respectively.

Comparison of the isotherms normalized at the maximum uptake of the different samples (Fig. 5) shows that the isotherms corresponding to the two encapsulated samples with the highest loadings overlap with that of the bare material while there is a slight deviation in the case of the 10 wt% encapsulated samples and larger deviations for the impregnated samples. Moreover, while the position of the characteristic steps of MIL-101 is the same for all the encapsulated samples and for the bare material, in the case of the impregnated samples, the second step almost disappears and the first one is shifted to lower pressures.

3.1.4. XRD

The XRD patterns of the different samples illustrated in Fig. 6 show hardly any difference between the bare sample of MIL-101(Cr) and the samples with the POM encapsulated. Apart from the fact that the intensity of the peak at 2 = 6° decreases for the encapsulated samples, the crystal structure seems to remain unchanged through the encapsulation of the POM, in clear contrast to the results reported by Sun et al. [18], where the encapsulation of POM in Cu-BTC produces a change in the MOF structure.

3.1.5. TGA

The thermo gravimetric analysis of the different catalysts in air is shown in Fig. 7. In every case water desorbs at around 100 °C. For the encapsulated samples (Fig. 7A), the maximum oxidation tem-

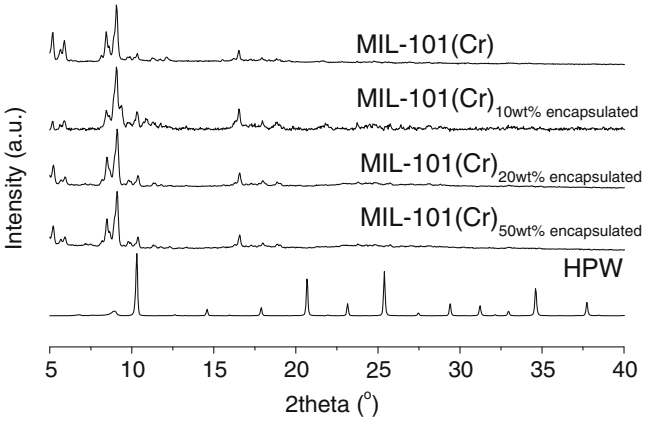

Fig. 6. X-ray diffraction patterns of the different encapsulated catalysts.

perature is lowered as the amount of POM in the sample increases. In contrast, the TGA curves for the POM impregnated samples (Fig. 7B) are similar to that for the bare material. These results strongly suggest a different nature and oxidation promotion of the encapsulated species.

3.1.6. Raman

Fig. 8 shows the spectra collected for the different MOF structures together with the spectrum corresponding to the bulk POM.

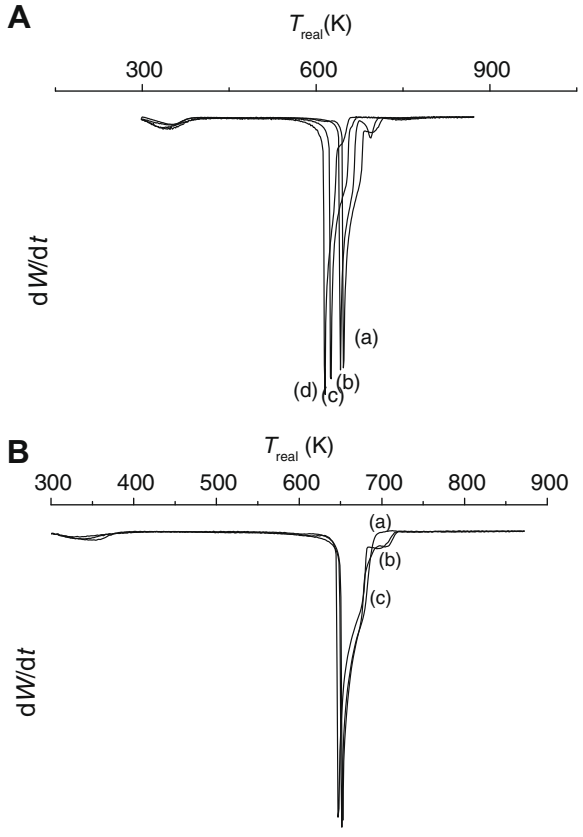

Fig. 7. DTG profiles of different MOFs in air at heating rate 10 K/min. (A) Comparison of different encapsulated POM loadings with bare MIL-101. (a) MIL-101(Cr); (b) MIL-101(Cr) with 10 wt% POM encapsulated; (c) MIL-101(Cr) with 20 wt% POM encapsulated; and (d) MIL-101(Cr) with 50 wt% POM encapsulated. (B) Comparison of different impregnated POM loadings with bare MIL-101. (a) MIL-101(Cr); (b) MIL-101(Cr) with 30 wt% POM impregnated; and (c) MIL-101(Cr) with 50 wt% POM impregnated.

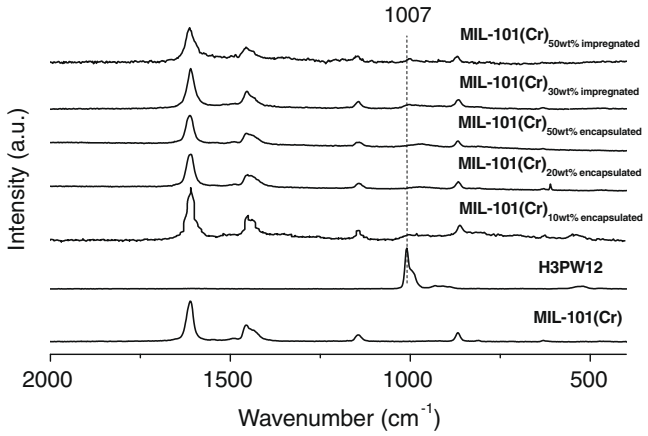

Fig. 8. Raman spectra of different MIL-101(Cr) encapsulated and impregnated POM samples.

Crystalline H_3PW shows characteristic bands at 1007 cm^{-1} (stretching vibration of P–O), 986 cm^{-1} (stretching of W=O), 900 cm^{-1} (bending of W–O_c–W), and 550 cm^{-1} (bending of O–P–O) [38]. Although the only visible bands in every case are the ones at 1007 and 986 cm^{-1}, some differences are also observed when comparing the encapsulated and impregnated samples. In the case of the encapsulated samples (Fig. 8A) the O–P–O and W=O bands are blue shifted by 15 wavenumbers, while for the impregnated samples (Fig. 8B) the stretching bands are not shifted with respect to the bare POM.

3.1.7. Drift

The DRIFT spectra of the different catalysts are shown in Fig. 9. Several differences are found when the bare sample is compared with the samples containing POM. The presence of strongly bonded water in the POM-containing samples may be clearly observed in Fig. 9A (range between 4000 and 800 cm^{-1}) from a broad absorption band between 3000 and 3500 cm^{-1}, the shoulder found at 1736 cm^{-1}, and the broad bands centered at 1294 cm^{-1} [39,40]. The last stretching band at 1294 cm^{-1} is also present in the bare sample; however, the intensity and width increase in the samples with POM. With respect to the OH stretchings of MIL-101 (3695 cm^{-1}), this band splits into two bands for the lower loaded POM samples (impregnated and encapsulated).

When focusing on the 800–1200 cm^{-1} region (Fig. 9B), several differences are found between the encapsulated and the impregnated catalysts: the MIL-101(Cr) band at 1163 cm^{-1} assigned to the Cr–O vibration is altered by the inclusion of POMs. In the case of the encapsulated samples, it becomes broader and the maximum shifts to lower wavenumbers for the low loaded samples, while it almost splits into two bands for the 50 wt% sample. In the case of the impregnated samples it becomes less intense. On the other hand, the bands corresponding to the W–O–W vibrations (895 and 900 cm^{-1}) appear in every sample containing POM, bands at 982 and 1080 cm^{-1} are clearer defined in the impregnated samples. The band at 982 cm^{-1} corresponds to the W=O stretching and is known to shift with the inclusion of 'addenda' metals or by changing the counter-cation [41]. The sharpness and exact position of the W=O are related to the content of water bonded to the POM structure and to the presence of addenda atoms: in Cr-containing phosphotungstic POMs the W=O stretching appears at 963 cm^{-1} [41]. The band at 1080 cm^{-1}, clearly present in the impregnated samples, is related to the P–O stretching in unsubstituted H_3PW. When addenda atoms like Cr^{3+} are added to the structure, this band tends to split into two vibrational absorption bands in the 1100 cm^{-1} area [41,42].

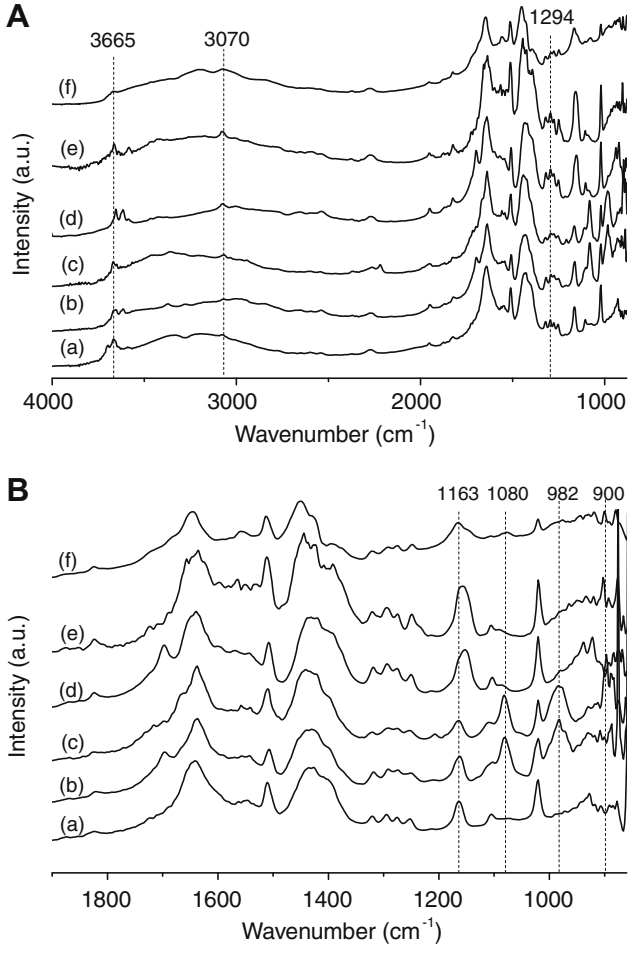

Fig. 9. DRIFT spectra of different MOFs. (a) MIL-101(Cr); (b) MIL-101(Cr) with 30 wt% POM impregnated; (c) MIL-101(Cr) with 50 wt% POM impregnated; (d) MIL-101(Cr) with 10 wt% POM encapsulated; (e) MIL-101(Cr) with 20 wt% POM encapsulated; and (f) MIL-101(Cr) with 50 wt% POM encapsulated.

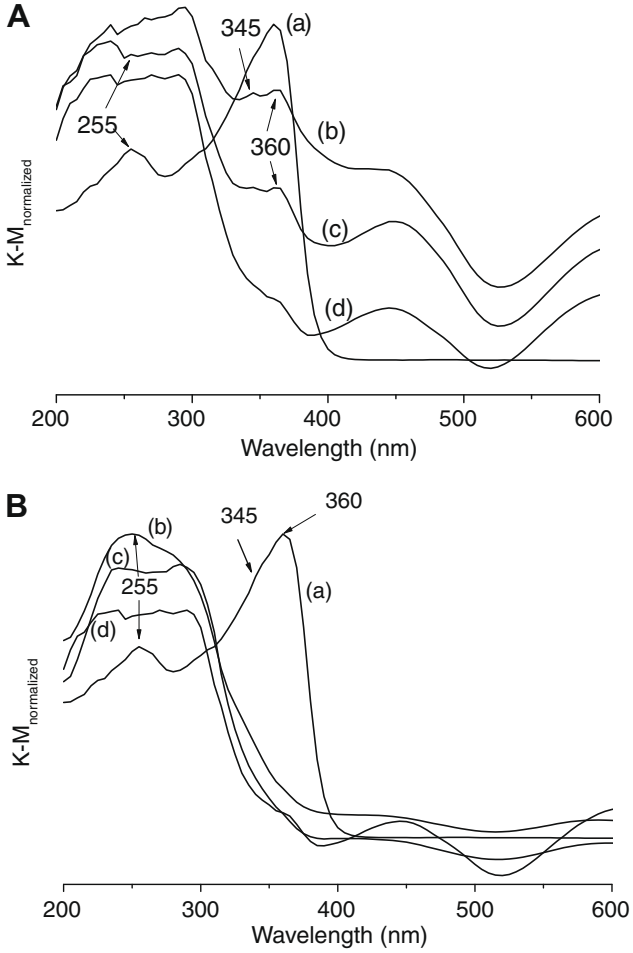

Fig. 10. UV–visible spectra of different MOFs. (A) Comparison of encapsulated samples. (a) POM spectrum; (b) MIL-101(Cr) with 50 wt% POM encapsulated; (c) MIL-101(Cr) with 20 wt% POM encapsulated; (d) MIL-101(Cr). (B) Comparison of impregnated samples. (a) POM spectrum; (b) MIL-101(Cr) with 50 wt% POM impregnated; (c) MIL-101(Cr) with 20 wt% POM impregnated; and (d) MIL-101(Cr).

3.1.8. UV–Visible

Fig. 10 compares the UV–Vis spectra in Kulbeka–Munk units of the different samples containing POM with the one of the bare MIL-101 and the bulk H_3PW.

Two main absorptions are present in the POM spectrum: the first is centered at 255 nm, and is attributed to the oxygen–tungsten charge-transfer absorption band for Keggin anions [43]. It is present in the H_3PW 50% impregnated and in the 20 wt% encapsulated sample, also clear in the 50 wt% encapsulated sample but shifted by 10 nm and it is absent in the 30% impregnated sample. The second broad absorption in the H_3PW is centered at 360 with a shoulder at 345 nm. For the encapsulated samples (Fig. 10A), these bands are clearly observed, whereas the spectra of the impregnated samples (Fig. 10B) do not show any difference with the one of the MIL-101 in this area. The MIL-101 band around 450 nm is even strongly decreased in these samples.

3.2. Catalytic performance

3.2.1. Knoevenagel condensation of benzaldehyde and ethyl cyanoacetate

3.2.1.1. Catalytic performance and influence of the solvent. The Knoevenagel condensation between benzaldehyde and ethyl cyanoacetate in toluene was selected as benchmark reaction to test the different MOFs. Although little has been published on the use of HPAs in this C–C bond formation reaction, recently Yoshida et al. utilized Knoevenagel condensation to benchmark the basic character of several lacunary HPAs [44].

The character of the solvent used in Knoevenagel condensations may have a strong effect on the reaction rate [45]. The polarity of the solvent affects the transition state and the capacity of the catalyst for proton transfer: when polar reagents are involved, the

Table 1
N_2-BET surface area calculated per grams of sample and per grams of MIL-101Cr (calculated between 0.05 and 0.15 relative pressures). Pore volume (calculated at 0.95–0.96 relative pressure) and final composition of the samples according to elemental analysis (POM percentage has been calculated considering 12 atoms of W per Keggin unit).

	S_{BET} [m^2/g_{solid}] (m^2/g_{MOF})	Pore volume [cm^3/g_{solid}] (cm^3/g_{MOF})	POM (wt%)	MIL-101(Cr) (wt%)
MIL-101(Cr)	2800	1.5	0	100
$MIL\text{-}101(Cr)_{10wt\%ENCAPSULATED}$	2340 (2600)	1.1 (1.2)	9.7	90.3
$MIL\text{-}101(Cr)_{20wt\%ENCAPSULATED}$	3047 (3809)	1.6 (2.0)	17.6	82.4
$MIL\text{-}101(Cr)_{50wt\%ENCAPSULATED}$	2445 (4890)	1.3 (2.6)	48.2	51.8
$MIL\text{-}101(Cr)_{50wt\%IMPREGNATED}$	1460 (2920)	0.7 (1.4)	50.3	49.7

transition-state complex is better solvated by polar solvents and the partition of the reactants at the solid-liquid interface is higher, decreasing the activation-free enthalpy and enhancing the reaction rate. Moreover, some protic solvents such as ethanol may also enhance the activation of the slightly acidic benzaldehyde, yielding a higher catalytic activity [22,45–47]. To avoid the promotion by the solvent, toluene (nearly apolar and non-protic) was chosen as a solvent for most of the catalytic tests, although also some experiments were performed using DMF (polar) and ethanol (protic and polar).

A fixed amount of catalyst was used in every case, implying different amounts of theoretically available active sites (i.e. 12/1000, 5/1000 or 2.5/100 molar ratio of acid groups in the MOF (50 wt%, 20 wt% and 10 wt%, respectively) to the amount of ethyl cyanoacetate used as a reactant for the encapsulated samples). The graphs presented in Figs. 11–13 show the evolution with time of the yield of ethyl (*E*)-α-cyanocinnamate based on the ethyl cyanoacetate conversion (100% selectivity was achieved in every case).

Fig. 11 shows the performance of different MOFs at 313 K using toluene as a solvent. 1,5,7-Triazabicyclo[4.4.0]dec-5-ene was used as a homogeneous catalyst under the same conditions in order to benchmark the activity of the synthesized catalyst with a well-known strong base [48]. Bulk POM was also tested, although no conversion could be achieved, since it is insoluble in toluene. The bare MIL-101(Cr) sample gave hardly any conversion either. The encapsulated samples are clearly much more active catalysts than those obtained by adsorption of the POM. While the impregnated POM sample yields 30% conversion after two reaction hours, the encapsulated POM catalysts reach values over 90%. The encapsulated samples exhibit also higher activities than the homogeneous base that reaches 45% conversion after two reaction hours.

Furthermore, while the activity of the 10 wt% and 20 wt% encapsulated samples is very similar, it is better than the 50 wt%, based on the amount of POM used.

A further insight into the catalytic process yields comparison of the turnover frequencies of the different catalysts at 313 K based on the theoretical number of active sites, mol POM or mol guanidine present (Table 2) and the conversion after 20 min. TOFs of 590 mol ECA/mol POM h^{-1} are obtained for the 10 wt% encapsulated sample, of the same order as the values found for the 20% encapsulated sample (420 h^{-1}) and far better than for the 50% encapsulated sample (138 h^{-1}).

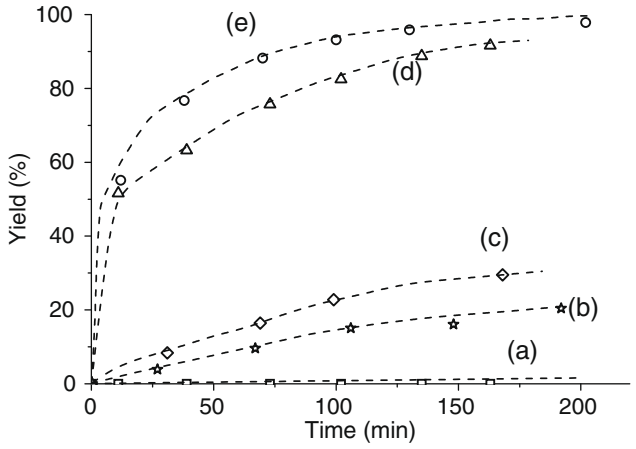

Fig. 11. Knoevenagel condensation of 8 mmol benzaldehyde and 7 mmol ethyl cyanoacetate over different MOF catalysts (0.5 g) in 5 mL of toluene as a solvent at 313 K. (a) MIL-101(Cr); (b) Bicycloguanidine (1,5,7-triazabicyclo[4.4.0]dec-5-ene); (c) MIL-101(Cr) with 50 wt% impregnated POM; (d) MIL-101(Cr) with 50 wt% POM encapsulated; and (e) MIL-101(Cr) with 20 wt% POM encapsulated.

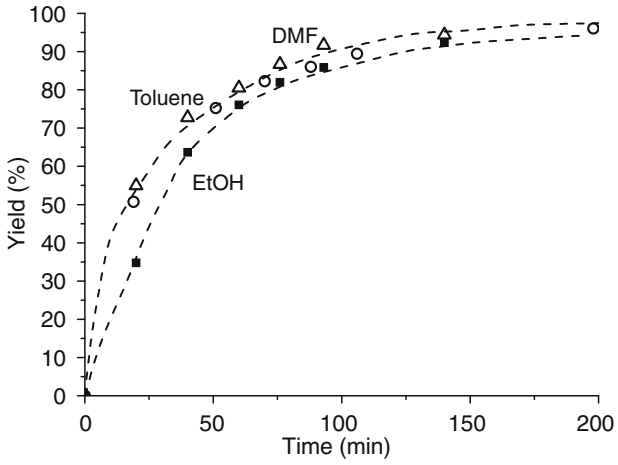

Fig. 12. Effect of the solvent on the performance of the catalyst (MIL-101(Cr)$_{10wt\%ENCAPSULATED}$) in the Knoevenagel condensation of 8 mmol benzaldehyde and 7 mmol ethyl cyanoacetate: 0.5 g catalyst, in 5 mL of solvent at 313 K.

Fig. 12 shows the performance of the 10 wt% encapsulated sample at 313 K when using different solvents: toluene, ethanol, and DMF under similar experimental conditions. In contrast to the common trend for this reaction, the activity of the catalyst is similar in DMF (non-protic, polar) and toluene (non-protic, nearly apolar), but is lower in ethanol (protic, polar). Indeed, while TOFs around 600 h^{-1} are found in DMF and toluene, values under 450 h^{-1} are found when using ethanol.

3.2.1.2. Re-usability and hot filtration experiments. Apart from presenting a good catalytic activity, long-term stability and the absence of leaching are of primary importance for solid catalysts. MOF samples were reused several times in order to determine if the catalysts suffer from permanent deactivation. The standard procedure, described in the experimental section, was followed to perform the first run. After 3 h of reaction the solid was filtered off and dried in an oven at 423 K overnight. Then the catalyst was tested in a second run using the same catalyst to reactants molar ratios. In some cases, catalysts were used in every reaction reported in this paper and afterwards re-used in a Knoevenagel condensation under standard conditions in order to demonstrate its full reusability. The possible leaching of the active phase was also studied by hot filtration experiments, the catalyst is filtered off during the reaction and possible catalytic activity in the obtained solution under the same conditions is followed.

Fig. 13 shows the catalytic activity of consecutive runs for every MOF as well as the hot filtration experiment. The sample with 20 wt% of POM encapsulated (Fig. 13A) exhibited the same catalytic activity in both runs, indicating no deactivation in both polar and non-polar solvents. After hot filtration of the catalyst (indicated by the arrow) no further reaction is observed in the solution, showing the heterogeneous behavior of the solids. Similar results were observed for the 50 wt% encapsulated sample (Fig. 13B) and for the 50 wt% impregnated sample (Fig. 13C). The hot filtration experiment for the latter type also confirms the absence of leaching, as indicated before in oxidation reactions [21,24]. Analysis of the liquid did not indicate any metal presence.

3.2.1.3. Unraveling the reaction mechanism. The Knoevenagel condensation may proceed according to two different mechanisms that depend on the nature of the catalyst. For strong bases, certain transition metal complexes (i.e. ruthenium) and strong Lewis acids, direct activation of the methylene group on the catalyst surface may take place. When weaker bases, such as amino groups are in-

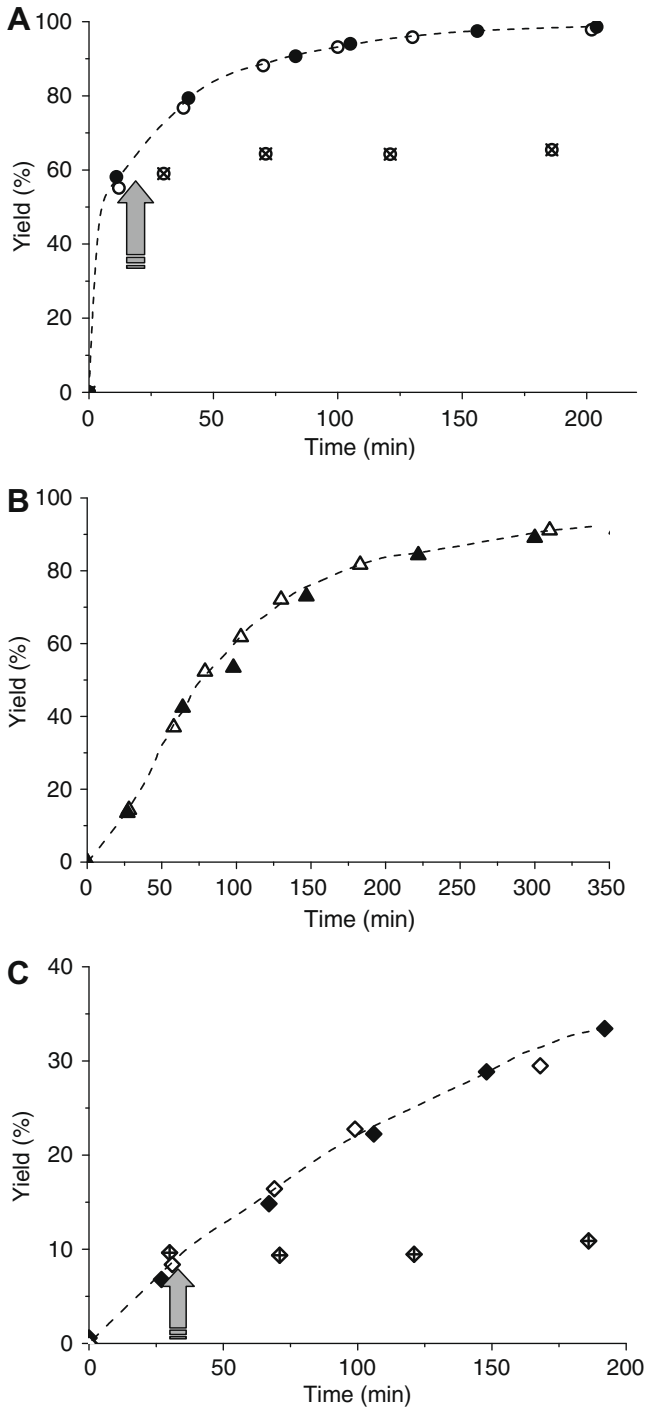

Fig. 13. Knoevenagel condensation of 8 mmol benzaldehyde and 7 mmol ethyl cyanoacetate in 5 mL of solvent at 313 K over different MOF catalysts. (A) MIL-101(Cr) with 20 wt% POM encapsulated in toluene. (○) 1st Run; (●) 2nd Run with a catalyst used in Knoevenagel condensation and esterification reactions; (⊗) hot filtration on a re-used (2×) catalyst. (B) MIL-101(Cr) with 20 wt% POM encapsulated in ethanol. (△) 1st run; (▲) 2nd run. (C) MIL-101(Cr) impregnated with 50 wt% POM in toluene. (◇) 1st run; (◆) 2nd run; (◈) hot filtration run. Arrow indicates moment of hot filtration.

volved in the catalytic process, the reaction proceeds through the formation of an imine intermediate: benzaldehyde reacts with an amino group to form a benzaldimine with a higher basicity than one of the free amine. Afterwards, the deprotonation of the methylene group takes place followed by the condensation, regenerating the active site [22,49].

Table 2
TON and TOF values obtained for the different catalysts in the Knoevenagel condensation of 8 mmol benzaldehyde and 7 mmol ethyl cyanoacetate over different MOF catalysts (mass: 0.5 g) in 5 mL of solvent at 313 K.

	Solvent	TON (t = 20 min)	TOF* (h^{-1})
MIL-101(Cr)$_{10wt\%ENCAPSULATED}$	DMF	216	>656
	Toluene	195	>591
	EtOH	146.7	445
MIL-101(Cr)$_{20wt\%ENCAPSULATED}$	Toluene	139	>420
MIL-101(Cr)$_{50wt\%ENCAPSULATED}$	Toluene	45	138
MIL-101(Cr)$_{50wt\%IMPREGNATED}$	Toluene	4	12
Bi-cyclo guanidine	Toluene	1.6	5

* Based on conversion after 20 reaction minutes.

With the aim of understanding why a catalyst with, in principle, only acid sites is able to perform in such outstanding way in a base-catalyzed reaction, the adsorption and activation of the active methylene compound (ethyl cyanoacetate) were followed *in situ* by FTIR. To this end, a solution of ethyl cyanoacetate in toluene (the same concentration as for the reaction experiments) was contacted in the cell with the MIL-101(Cr)$_{20\%ENCAPSULATED}$ sample and the evolution of its IR spectra was followed while increasing the temperature in the DRIFTcell. The results are plotted in Fig. 14.

After contacting at room temperature the solution of ethyl cyanoacetate with the MOF encapsulated sample, all the main vibrations from the active methylene compound are present while the catalyst bands related to the OH (3700 cm^{-1}) and Cr–O (1163 cm^{-1}) stretchings disappear. Upon raising the temperature, the formation of CO_2 is evident from the appearance of a new band at 2318 cm^{-1}. At the highest temperature, a new band appears at 2212 cm^{-1} while the ethyl cyanoacetate and CO_2 bands disappear and the catalyst vibrations are recovered. Similar DRIFTS experiments performed with a mixture of benzaldehyde and toluene revealed no chemical interaction with the catalysts (not shown). These results suggest a strong interaction between the active methylene compound and the encapsulated sample.

3.2.2. Esterification of n-butanol and acetic acid

The esterification of *n*-butanol with acetic acid was chosen to test the different catalysts in a liquid phase acid-catalyzed reaction. The acetic acid – *n*-butanol molar ratio was 1:1. A total of 3 g of catalyst per mol of acetic acid or *n*-butanol was used, this amount corresponds with 0.036 mmol (0.5 g) of POM in the 20 wt% of POM encapsulated sample used. Fig. 15 shows the yield of butyl acetate based on the acetic acid conversion (100% selectivity) as a function of time at 383 K.

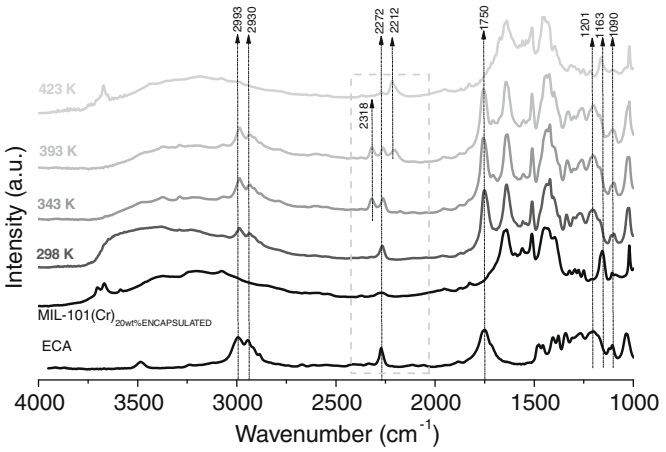

Fig. 14. DRIFTs spectra of activated MIL-101(Cr)$_{20\%ENCAPSULATED}$ after contacting with a solution of ethyl cyanoacetate in toluene (1.4 mol/l) at different temperatures.

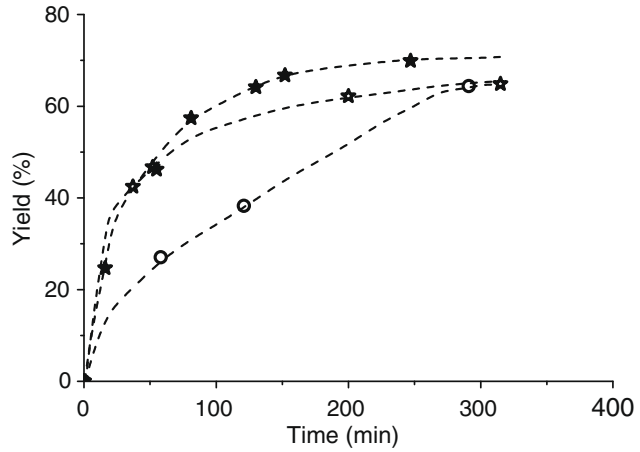

Fig. 15. Esterification of acetic acid with *n*-butanol (molar ratio 1:1) at 383 K with 3 g of catalyst per mol of acetic acid. Yield of ester as a function of time. (○) MIL-101(Cr) with 20 wt% POM encapsulated; (☆) 0.6 g POM (equivalent to 20 wt% MIL-101 sample); (★) Nafion NR50.

The best catalytic activity was presented by the 20 wt% POM encapsulated sample, and it has been compared with that of dissolved POM acting as a homogeneous catalyst (the same amount used as present in the MOF sample) and the performance of both has been benchmarked with Nafion NR 50 (the same mass of resin as MOF sample). While experiments performed with the 10% and 50% encapsulated catalysts showed conversions in the range of 50% after five reaction hours, the experiments with the impregnated POM samples did not show any differences with the blank runs (20% conversion after 5 h).

In all other cases equilibrium is almost reached after 300 min. Both the Nafion and the dissolved POM present a higher reaction rate.

TON and TOF values were calculated for both POM-based catalysts: The 20 wt% of POM encapsulated sample presents a TON higher than 3000 and a TOF value around 11 h^{-1}, higher than those reported in the literature for POM immobilized on other mesoporous supports under similar reaction conditions [31].

3.2.3. Dehydration of Methanol to DME

The dehydration of methanol to DME is a gas phase reaction also catalyzed by acids. The conversion and selectivity to DME at different temperatures are shown in Fig. 16 for three weight hourly space velocities (WHSVs) for the 20 wt% encapsulated sample. Conversion is given after 30 reaction minutes, no deactivation of the catalyst was observed during the experiments.

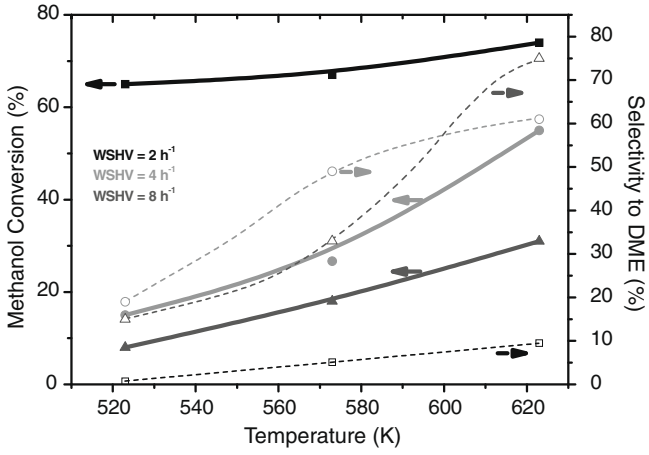

Fig. 16. Methanol conversion and selectivity to DME in the dehydration of methanol as a function of temperature at different weight hourly space velocities. Catalyst: 100 mg of MIL-101(Cr)$_{20wt\%ENCAPSULATED}$. Molar feed ratio N_2:MeOH = 5:1. Closed symbols: conversion, Open symbols: selectivity. WHSV = 2(□), 4(○) and 8(◇) h^{-1}.

At WHSV = 2 h^{-1} methanol conversion levels of ~70% and very low DME selectivities are achieved over the whole temperature range. When increasing the WHSV (4 h^{-1}) both selectivity and conversion increase with temperature. At the highest WHSV (8 h^{-1}) conversion is the lowest, but at the highest temperature the selectivity is the highest.

4. Discussion

The HRTEM analysis (Fig. 2) confirms that the direct encapsulation of POM in MIL-101(Cr) is possible through the addition of acid to the synthesis mixture and subsequent hydrothermal treatment, as already shown by Sun et al. for another MOF structure, HKUST-1 [18]. Stirring the reaction mixture during the synthesis, however, improves dramatically the distribution of the POM in the MIL-101 matrix, as shown by the EDX analysis and the EDS mapping of Figs. 2 and 4, and the resulting catalytic performance (Figs. 11–14).

Although no TEM pictures were shown by Sun et al., a comparison of their results with this work should be done with caution because of several reasons: the topology of the host MOFs is different: in the case of CuBTC only one Keggin unit can be allocated in every large cavity, while in the case of MIL-101 the mesoporous cavities are much bigger and more Keggin units may be accommodated per cavity. This fact may account for the necessity of stirring (rotational synthesis) in the case of MIL-101 to avoid the formation of concentration gradients in the synthesis vessel.

The better dispersion of the POM when directly encapsulated compared to the impregnated samples is demonstrated by the comparison of the different N_2 isotherms (Fig. 5). The two characteristic steps in the MIL-101 isotherms are related with the filling of the mesoporous cavities. At very low relative pressures ($P/P^0 < 0.05$) only the supertetrahedra are filled. As pressure increases, the medium ($P/P^0 = 0.15$) and later the large cavities ($P/P^0 = 0.20$) are filled [37]. The fact that the encapsulated samples with high POM loadings show an adsorptive behavior similar to that of the bare material strongly suggests that the filling of the cavities by the POM molecules is quite homogeneous. Apparently, the arrangement of the POM in the impregnated samples is quite different: the ratio between the adsorbed amount of N_2 at low relative pressures (adsorption in the supertetrahedra) and the adsorbed amount at higher relative pressures (adsorption in the cavities) is relatively larger than for the bare MIL-101. It means that only a smaller fraction of the cavities is filled with POM and that most of these –*large*– cavities are blocked. In contrast, when encapsulated, the POM molecules may also be present in the medium-sized cavities through the direct synthesis, unlike after the post-impregnation treatment since they are too big to enter through the pentagonal windows (Fig. 1). A much better dispersion results for the encapsulated samples, there is no indication of blocking of the cavities at all. Considering the amount of POM incorporated into the MIL-101, on average about 5.3 Keggin units should be present in every large cavity of the 50 wt% impregnated sample [24] and up to two units would be present per cavity (medium and large) for the same loading on a encapsulated sample. Considering the volumes of a Keggin unit (2250 $Å^3$) and the volume of the MIL-101 cages (20,600 and 12,700 $Å^3$, respectively), the difference in the adsorptive behavior between the encapsulated and the impregnated samples is not surprising: the volume of six Keggin units, even if they are very close to each other, may block completely a large cavity or at least block some of the windows of such cavity. In the case of the other encapsulated samples, approxi-

mately one Keggin unit would be present in every cavity of the 20 wt% while only half the cavities would be occupied by POM for the 10 wt% sample. This fact accounts for the differences found in the shape of the N_2 isotherms between the lowest loaded sample (10 wt%) and the other encapsulated samples. A 10 wt% is not enough to fill every cavity, resulting in empty spaces and therefore different isotherms.

All samples synthesized showed the XRD pattern of pure MIL-101, while no reflections corresponding to the bulk POM were detected, demonstrating the absence of large POM crystals in the outer surface of the particles. Moreover, the higher background appearing in the 10% encapsulated sample suggests an irregular occupation of the cavities, since only half of the cavities can be occupied by this low amount of Keggin units.

With respect to the nature of the encapsulated species, every spectroscopic evidence points in the same direction: structural changes in the original Keggin H_3PW unit have taken place during the encapsulation process. The stabilization of lacunary POMs through exchange of tungsten with other transition metals has been widely reported in the literature [34,44,50,51]. Metal-substituted polyoxometalates contain transition metals as addenda ions. The transition metal fits into the lacunary vacancy created in the otherwise complete Keggin structural unit. The lacunary or "defect structure" is created by the loss of an MO_6 octahedron (which is equivalent to stoichiometric loss of a MO^{n+} unit resulting in the formation of $XM_{11}O_{39}^{n-}$) [30]. Although these species are usually synthesized at higher pH (2–3) than during the synthesis of MIL-101 (pH < 1), at high temperatures Cr^{3+} may be incorporated in the Keggin structure.

Furthermore, Cr^{3+}-substituted POMs have been reported to be excellent oxidation catalysts [41,42]. TG analysis confirms that the oxidation temperature of the encapsulated samples depends on the amount of POM, whereas the impregnated samples show oxidation profiles similar to the bare MIL-101. Although the incorporation of W into the framework cannot be discarded, in this case we would expect changes in the positions of the main XRD reflexions that are not observed.

UV–Vis spectroscopy shows clear evidences of the presence of POMs. The peak centered at 255 nm is attributed to the oxygen–tungsten charge-transfer for Keggin anions [52]. This transition is clearly observed in the 50 wt% impregnated samples, and it is also present in every encapsulated sample, although the intensity is weaker. This fact suggests that at least a part of the Keggin molecules is intact after direct inclusion in the porous structure. The new absorption bands appearing at 360 and 345 nm can be related to interactions Cr–O–W, in analogy to Fe-containing POMs [51]. Meaning that part of the POM introduced is modified during the synthesis and some W atoms are being substituted by Cr^{3+} forming the corresponding lacunary structures ($[PW_{11}O_{39}Cr(H_2O)]^{4-}$, $[(PW_{11}O_{39}Cr)_2O]^{10-}$, ($[PW_{11}O_{39}Cr(OH)]^{5-}$) [41,42].

DRIFTs yields additional information for the exchange with Cr. Upon comparing the encapsulated samples with the impregnated samples, the first main difference is the distortion appearing in the OH bands of MIL-101 (3665 cm^{-1}) together with the new bands appearing in the encapsulated samples at around 3070 cm^{-1}. The distortion in the first one is an evidence of the interaction between the guest species and the framework, while the appearance of the last one may be related to the presence of water ligands, which is much more evident in the case of the 50 wt% and hardly present in the case of the 10 wt% encapsulated samples and that corresponds to the formation of sandwich-like structures between several $[PW_{11}O_{39}Cr(H_2O)]^{4-}$ lacunary subunits [44].

With respect to the main IR absorption vibrations of the POM, there is a large difference in the relative intensities of the bands and some of them are shifted in the encapsulated samples. The W=O stretching appears as a very broad band centered at 982 cm^{-1} for the impregnated POM catalysts. In the case of the encapsulated catalysts this band is weaker and less broad, and moreover a new band appears at 963 cm^{-1}. This stretching has been reported for Cr(III) containing lacunary $PW_{11}O_{39}^{7-}$ [41]. The P–O vibration appears at 1080 cm^{-1} for all the samples and corresponds to the PO_4 units of the symmetric $PW_{12}O_{40}^{3-}$ anion. The fact that the 1080 cm^{-1} band is less intense in the encapsulated samples is also related with the fact that a part of the H_3PW has been exchanged with Cr^{3+} during the encapsulation, producing an asymmetry in the PO_4 environment and therefore the splitting of a single band into several ones. Moreover, the MIL-101(Cr) band at 1163 cm^{-1} assigned to the Cr–O vibration is altered by the encapsulation of POMs also suggest the existence of further Cr–O vibrations, or even to a second P–O vibration in the presence of Cr^{3+} [41,51].

The different nature of the POMs in the solids couples with the catalytic results. The encapsulated samples have been shown to be very active in the Knoevenagel condensation and quite active in the esterification reaction, while the impregnated samples show only a fair activity in the Knoevenagel and hardly any activity in the esterification. The latter has to be related with a stronger interaction (MOF) – POM and POM–POM when the active species are post-synthetically introduced (impregnated) and with the different nature of the active species. The stronger interaction of the acid with the MOF when impregnated can be deduced from the disappearance of the 460 nm UV–Vis band of MIL-101 for these samples while it remains intact for the encapsulated samples. Indeed, Ferey et al. already reported the absence of counter anions (potassium) inside the MOF structure when impregnating the K-salt of the Keggin species, which is another evidence of a strong electrostatic interaction acid–support. It is well known that H_3PW is active when immobilized on several supports, but with increasing strength of the acid–support interaction, the acidity decreases dramatically, like for activated carbons [53]. Moreover, the presence of more Keggin units per cavity might lead to stronger POM–POM interactions and to accessibility issues not present in the better dispersed encapsulated samples.

The catalysts are fully reusable and no activity loss was observed during consecutive tests (Fig. 12), some samples were reused up to eight times in different reactions (corresponding with a total TON > 3000 for 10 wt% encapsulated sample). The absence of leaching is concluded from the hot filtration experiments, and the absence of tungsten in the reaction medium is concluded from elemental analysis after reactions in polar (*n*-butanol) and non-polar (toluene) media.

The performance of the encapsulated samples in the Knoevenagel condensation is outstanding when using different toluene and DMF as a solvent, and is very good when using a polar solvent such as ethanol [22,46,47]. The most active catalysts are the ones with the lowest loadings, the 10 wt% and 20 wt% encapsulated MIL-101's: almost 100% of conversion is reached after two reaction hours (Fig. 11). When comparing the turnover frequencies the lower loading samples are three times more active than the 50 wt% encapsulated sample, 30 times more than the impregnated sample, and over 100 times more active than the bicyclo guanidine, which is state-of-the-art organic base [48].Neither the bulk POM (insoluble) nor the bare MIL-101(Cr) showed any activity under the applied conditions.

We speculate that the mechanism of the Knoevenagel condensation is similar to the one shown by certain metallic complexes and some strong Lewis acids (see Scheme 1) [54]: coordination of the nitrile to a lacunary site and subsequent proton abstraction. The addition of the lacunary site to the C–H bond of the nitrile affords a hydrido a-cyanoalkyl complex, which is converted into a stable hydrido(enolato)-complex (A). Direct interaction of A with

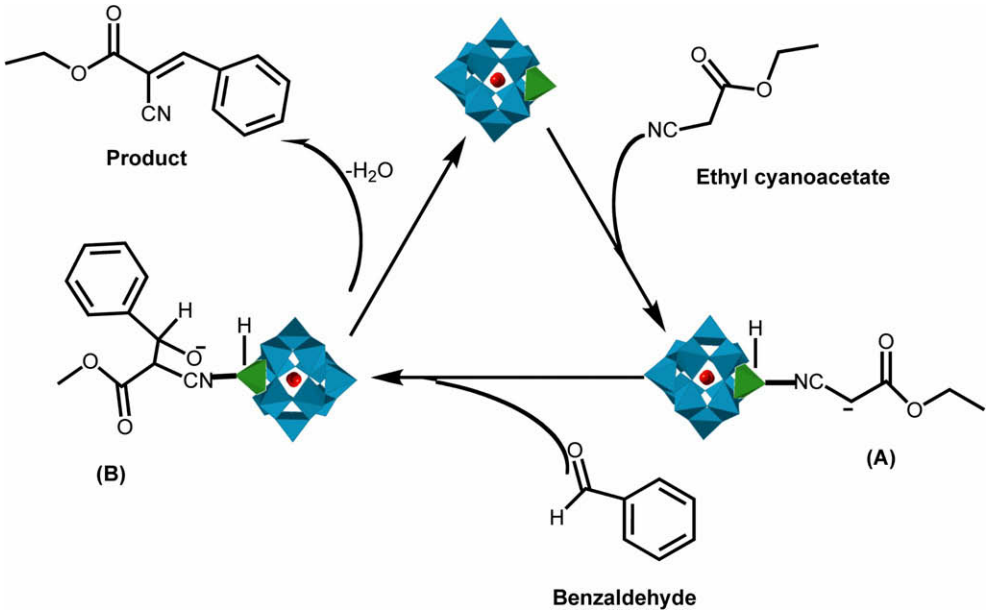

Scheme 1. Proposed reaction mechanism for the Knoevenagel condensation (blue: tungsten, green: chromium, and red: oxygen). (For interpretation of the references to colour in this figure legend, the reader is referred to the web version of this article.)

benzaldehyde would take place to give hydrido(aldolato)-(B) intermediate, which undergoes elimination of aldol product to close the catalytic cycle. When no aldehyde is present (Fig. 13), the hydrido(enolato)-complex (A) can be broken by raising the temperature, liberating CO_2 (band at 2318 cm^{-1}), and producing the condensation of CN units on the active sites (band at 2212 cm^{-1}).

According to the proposed mechanism, the lower activity shown in ethanol, may be explained by the fact that both the alcohol and the water formed during the reaction (miscible with the alcohol) would compete with the ethyl cyanoacetate for the active "*basic*" sites, resulting in a lower reaction rate.

The activity shown in acid catalysis by the best-dispersed (encapsulated) samples is remarkable. They are active in the dehydration of methanol to DME at moderate reaction conditions, although a low selectivity to DME is obtained in comparison with other acid solids [55–57]. This is related with the formation of longer chain hydrocarbons that adsorb in the MIL-101 cavities. Indeed, the presence of negatively charged active sites together with large specific surface areas is not the best combination for reactions like DME formation.

In the case of the esterification, although the initial activity is lower than the homogeneous POM counterpart on a molar basis and than the Nafion on a total weight basis, the encapsulated sample shows TONs similar to those of other supported POM catalysts on mesoporous silicas [31], demonstrating the presence of purely acid sites within the catalysts.The combined interpretation of the different catalytic results together with the characterization performed results in the next overall picture:

- During the one-pot synthesis, tungsten is partially exchanged by chromium. As result of this exchange lacunary polyoxometalates are encapsulated by the cavities of MIL-101.
- The best catalytic performance, on a weight basis, is obtained for catalysts containing less than 1 POM molecule per MIL-101 cavity (10 wt% and 20 wt%). For higher loadings of POM, not all the sites are accessible for the large molecules like the ones involved in the Knoevenagel condensation. On the other hand, the lower total oxidation temperature shown in the TGA analysis demonstrates the accessibility of these sites for smaller molecules such as O_2.
- The large density of lacunary sites explains the outstanding performance in the Knoevenagel condensation of ethyl-cyanoacetate with benzaldehyde.
- In spite of the presence of lacunary sites, the partial integrity of the initial Brønsted acid Keggin units is demonstrated by the activity shown in the esterification and in the dehydration of methanol.

To summarize, we have reported the synthesis of a new class of porous solids with an outstanding bi-functional catalytic activity. Moreover, the facile one-pot synthesis is preferred over multi-step preparation procedures. The application of this new class of catalysts in other reactions involving proton abstraction, oxidation, polymerization, alkylation, and collaborative or tandem catalysis is under study and their performance will be reported soon.

5. Conclusions

The addition of phosphotungstic acid to the synthesis mixture of MIL-101(Cr) yields the direct encapsulation of polyoxometalates of different nature into the MOF structure.

Vibrational spectroscopies evidence the partial substitution of tungsten by Cr^{3+} in the POM, forming the so-called lacunary structures.

An excellent dispersion of the active species over the sample is obtained when combining the one-pot approach with synthesis under rotating conditions. N_2 adsorption results suggest that the ratio of medium to large cavities occupied by the POM is similar to the ratio in the bare MIL-101, demonstrating that both the large- and the medium-sized cavities may be used as host for relatively large species, unlike when using impregnation where only the larger cavities are accessed.

The performance of these new catalysts in the Knoevenagel condensation of benzaldehyde and ethyl cyanoacetate is outstanding. No catalyst showing such high activity at 313 K both in an apolar and in a polar solvent has been reported in the literature so far.

The stabilization of lacunary POMs in MOF matrices may represent a new generation of catalysts with a high proton abstraction capability.

The encapsulated catalysts show a remarkable activity in acid-catalyzed reactions, demonstrating the bi-functionality of these solids. In the catalysts prepared by impregnation, the strong interaction POM–support deteriorates the acidity of the resulting solid, and hence the catalytic activity.

Acknowledgments

The Delft University of Technology is gratefully acknowledged for financial support provided to JJ-A and EVR-F. J.G. gratefully acknowledges the Netherlands National Science Foundation (NWO) for his personal VENI grant. Ir. Frans van Oostrum is acknowledged for performing the SEM-EDS measurements. The Department of Materials Science and Engineering of the Delft University of Technology is acknowledged for performing the XRD analyses. Ir. Yasukasu Kumita is gratefully acknowledged for his help in the methanol dehydration experiments. Prof. Em. Dr. Ir. Herman van Bekkum and Prof. Dr. Ulf Hanefeld are gratefully acknowledged for fruitful discussions.

References

[1] J.R. Long, O.M. Yaghi, Chem. Soc. Rev. 38 (2009) 1213–1214.
[2] J.J. Perry, J.A. Perman, M.J. Zaworotko, Chem. Soc. Rev. 38 (2009) 1400–1417.
[3] G.K.H. Shimizu, R. Vaidhyanathan, J.M. Taylor, Chem. Soc. Rev. 38 (2009) 1430–1449.
[4] D.J. Tranchemontagne, J.L. Mendoza-Cortes, M. O'Keeffe, O.M. Yaghi, Chem. Soc. Rev. 38 (2009) 1257–1283.
[5] M.D. Allendorf, C.A. Bauer, R.K. Bhakta, R.J.T. Houk, Chem. Soc. Rev. 38 (2009) 1330–1352.
[6] M. Kurmoo, Chem. Soc. Rev. 38 (2009) 1353–1379.
[7] L.J. Murray, M. Dinca, J.R. Long, Chem. Soc. Rev. 38 (2009) 1294–1314.
[8] J.R. Li, R.J. Kuppler, H.C. Zhou, Chem. Soc. Rev. 38 (2009) 1477–1504.
[9] S. Couck, J.F.M. Denayer, G.V. Baron, T. Remy, J. Gascon, F. Kapteijn, J. Am. Chem. Soc. 131 (2009) 6326–6327.
[10] D. Farrusseng, S. Aguado, C. Pinel, Angewandte Chemie International Edition, vol. 9999 (2009) NA.
[11] J. Lee, O.K. Farha, J. Roberts, K.A. Scheidt, S.T. Nguyen, J.T. Hupp, Chem. Soc. Rev. 38 (2009) 1450–1459.
[12] M.H. Alkordi, Y. Liu, R.W. Larsen, J.F. Eubank, M. Eddaoudi, J. Am. Chem. Soc. 130 (2008) 12639–12641.
[13] Do-Young Hong, Young Kyu Hwang, Christian Serre, Gerard Ferey, Jong-San Chang, Adv. Funct. Mater. 19 (2009) 1537–1552.
[14] S. Hasegawa, S. Horike, R. Matsuda, S. Furukawa, K. Mochizuki, Y. Kinoshita, S. Kitagawa, J. Am. Chem. Soc. 129 (2007) 2607–2614.
[15] L.Q. Ma, C. Abney, W.B. Lin, Chem. Soc. Rev. 38 (2009) 1248–1256.
[16] J.S. Seo, D. Whang, H. Lee, S.I. Jun, J. Oh, Y.J. Jeon, K. Kim, Nature 404 (2000) 982–986.
[17] J. Gascon, M.D. Hernandez-Alonso, A.R. Almeida, G.P.M. van Klink, F. Kapteijn, G. Mul, ChemSusChem 1 (2008) 981–983.
[18] C.-Y. Sun, S.-X. Liu, D.-D. Liang, K.-Z. Shao, Y.-H. Ren, Z.-M. Su, J. Am. Chem. Soc. 131 (2009) 1883–1888.
[19] F.X. Llabres i Xamena, A. Abad, A. Corma, H. Garcia, J. Catal. 250 (2007) 294–298.
[20] F.X. Llabrés i Xamena, O. Casanova, R. Galiasso Tailleur, H. Garcia, A. Corma, J. Catal. 255 (2008) 220–227.
[21] N.V. Maksimchuk, M.N. Timofeeva, M.S. Melgunov, A.N. Shmakov, Y.A. Chesalov, D.N. Dybtsev, V.P. Fedin, O.A. Kholdeeva, J. Catal. 257 (2008) 315–323.
[22] J. Gascon, U. Aktay, M.D. Hernandez-Alonso, G.P.M. van Klink, F. Kapteijn, J. Catal. 261 (2009) 75–87.
[23] X. Zhang, F.X. LlabrÈs i Xamena, A. Corma, J. Catal. 265 (2009) 155–160.
[24] G. Ferey, Science 310 (2005) 1119.
[25] P. Horcajada, S. Surble, C. Serre, D.Y. Hong, Y.K. Seo, J.S. Chang, J.M. Greneche, I. Margiolaki, G. Ferey, Chem. Commun. (2007) 2820–2822.
[26] C. Serre, F. Millange, C. Thouvenot, M. Nogues, G. Marsolier, D. Louer, G. Ferey, J. Am. Chem. Soc. 124 (2002) 13519–13526.
[27] S. Surble, C. Serre, C. Mellot-Draznieks, F. Millange, G. Ferey, Chem. Commun. (2006) 284–286.
[28] S.H. Jhung, J.H. Lee, J.W. Yoon, C. Serre, G. Ferey, J.S. Chang, Adv. Mater. 19 (2007) 121.
[29] A. Henschel, K. Gedrich, R. Kraehnert, S. Kaskel, Chem. Commun. (2008) 4192–4194.
[30] I.V. Kozhevnikov, Chem. Rev. 98 (1998) 171–198.
[31] S.S. Wu, J. Wang, W.H. Zhang, X.Q. Ren, Catal. Lett. 125 (2008) 308–314.
[32] H. Atia, U. Armbruster, A. Martin, J. Catal. 258 (2008) 71–82.
[33] M.A. Schwegler, P. Vinke, M. van der Eijk, H. van Bekkum, Appl. Catal. A: Gen. 80 (1992) 41–57.
[34] J. Haber, K. Pamin, L. Matachowski, D. Mucha, Appl. Catal. A: Gen. 256 (2003) 141–152.
[35] I.V. Kozhevnikov, A. Sinnema, R.J.J. Jansen, K. Pamin, H. Bekkum, Catal. Lett. 30 (1994) 241–252.
[36] P. Ferreira, I.M. Fonseca, A.M. Ramos, J. Vital, J.E. Castanheiro, Catal. Commun. 10 (2009) 481–484.
[37] P.L. Llewellyn, S. Bourrelly, C. Serre, A. Vimont, M. Daturi, L. Hamon, G. De Weireld, J.S. Chang, D.Y. Hong, Y.K. Hwang, S.H. Jhung, G. Ferey, Langmuir 24 (2008) 7245–7250.
[38] E. Caliman, J.A. Dias, S.C.L. Dias, A.G.S. Prado, Catal. Today 107–08 (2005) 816–825.
[39] P.Y. Vuillaume, A. Mokrini, A. Siu, K. Théberge, L. Robitaille, Eur. Polym. J. 45 (2009) 1641–1651.
[40] A.M. Herring, R.L. McCormick, J. Phys. Chem. B 102 (1998) 3175–3184.
[41] N.I. Kuznetsova, L.I. Kuznetsova, V.A. Likholobov, J. Mol. Catal. A: Chem. 108 (1996) 135–143.
[42] L.I. Kuznetsova, L.G. Detusheva, N.I. Kuznetsova, M.A. Fedotov, V.A. Likholobov, J. Mol. Catal. A: Chem. 117 (1997) 389–396.
[43] M.H. Youn, H. Kim, J.C. Jung, I.K. Song, K.P. Barteau, M.A. Barteau, J. Mol. Catal. A: Chem. 241 (2005) 227–232.
[44] A. Yoshida, S. Hikichi, N. Mizuno, J. Organomet. Chem. 692 (2007) 455–459.
[45] A. Corma, S. Iborra, I. Rodriguez, F. Sanchez, J. Catal. 211 (2002) 208–215.
[46] M.J. Climent, A. Corma, I. Dominguez, S. Iborra, M.J. Sabater, G. Sastre, J. Catal. 246 (2007) 136–146.
[47] I. Rodriguez, G. Sastre, A. Corma, S. Iborra, J. Catal. 183 (1999) 14–23.
[48] Y.V.S. Rao, D.E. De Vos, P.A. Jacobs, Angew. Chem., Int. Ed. 36 (1997) 2661–2663.
[49] S.I. Murahashi, T. Naota, H. Taki, M. Mizuno, H. Takaya, S. Komiya, Y. Mizuho, N. Oyasato, M. Hiraoka, M. Hirano, A. Fukuoka, J. Am. Chem. Soc. 117 (1995) 12436–12451.
[50] M.W. Droege, R.G. Finke, J. Mol. Catal. 69 (1991) 323–338.
[51] K. Nowinska, M. Sopa, A. Waclaw, D. Szuba, Appl. Catal. A: Gen. 225 (2002) 141–151.
[52] Chunfeng Shi, Runwei Wang, Guangshan Zhu, Shilun Qiu, Jun Long, Eur. J. Inorg. Chem. 2005 (2005) 4801–4807.
[53] T. Okuhara, N. Mizuno, M. Misono, Adv. Catal. 41 (41) (1996) 113–252.
[54] R.A. Sheldon, H.v. Bekkum, Fine Chemicals through Heterogeneous Catalysis, Wiley-VCH, 2001, ISBN:3-527-29951-3.
[55] J. Khom-In, P. Praserthdam, J. Panpranot, O. Mekasuwandumrong, Catal. Commun. 9 (2008) 1955–1958.
[56] F. Raloof, M. Taghizadeh, A. Eliassi, F. Yaripour, Fuel 87 (2008) 2967–2971.
[57] F. Yaripour, A. Mollavali, S.M. Jam, H. Atashi, Energy Fuels 23 (2009) 1896–1900.